JOURNAL OF PROPULSION AND POWER
Vol. 16, No. 2, March–April 2000

Confined Swirling Flows with Heat Release and Mixing

David S. Underwood,* Ian A. Waitz,† and Edward M. Greitzer‡
Massachusetts Institute of Technology, Cambridge, Massachusetts 02139

A simplified model is used to illustrate global features and flow regimes encountered in swirling flows with combustion, as an approach to providing an overall interpretation of the behavior of primary zone flows in lean-premixed-prevaporized gas turbine combustors. As one example of this, the physical mechanisms that characterize the interactions between swirl and heat addition are described, including the differing effects on recirculation zone formation for low and high values of swirl. The model, which is based on a quasi-one-dimensional control volume formulation, contains many approximations for the relevant flow processes. Nevertheless, comparisons of this simplified model with results from an axisymmetric Navier–Stokes code support the utility of the approach for gaining physical insight into the overall behavior of these parametrically complex flows.

Nomenclature

A = control volume area
b' = planar shear layer growth rate
C_p = specific heat of air at constant pressure
E = Eckert number, $(u_1 - u_2)^2 / Cp_t T_1$
h = enthalpy
L = duct length
M = Mach number
$\mathcal{M}$ = momentum, $\dot{m}u$
$\dot{m}$ = mass flow
Pr_t = turbulent Prandtl number
p = static pressure
R = radius of duct
Re_b = Reynolds number based on shear layer thickness, $\Delta U b / \nu_t$
r = velocity ratio, u_1 / u_2
s = density ratio, ρ_1 / ρ_2
T = static temperature
$\bar{U}$ = average axial velocity of core and outer streams
u = velocity in axial direction
v = velocity in circumferential direction
w = velocity in radial direction
z = coordinate in axial direction
α = area ratio, A_D / A_1
Γ = circulation
ΔU = velocity difference, $u_1 - u_2$
δ = radius of vortex core
η = ratio of specific heats at constant pressure, C_{p_1} / C_{p_2}
ν_t = effective turbulent viscosity
Ξ = mixing coefficient
ρ = density
τ = temperature ratio, T_1 / T_2
ϕ = equivalence ratio
Ω = swirl ratio, $\Gamma / 2\pi \delta u_1$

Subscripts

c = centerline
D = duct
m = mixing
pr = product formation due to chemical reaction
1 = vortex core
2 = irrotational outer stream

Received 8 October 1997; revision received 20 February 1999; accepted for publication 1 March 1999.

*Graduate Research Assistant, Gas Turbine Laboratory, 31-256 MIT.
†Associate Professor, Aeronautics and Astronautics, Gas Turbine Laboratory, 31-266 MIT.
‡Professor, Aeronautics and Astronautics, Gas Turbine Laboratory, 33-207 MIT.

I. Introduction

THE behavior of gas turbine combustor primary zone flows impacts ignition, stability, efficiency, and pollutant formation. Primary zones are typified by swirling flow with heat release in a variable area duct, where a central toroidal recirculation zone is formed. The recirculation zone allows the mixing of hot products with incoming reactants, thereby anchoring the flame.

The work presented in this paper focuses on lean-premixed-prevaporized (LPP) combustor technology, which has proven effective in reducing NO_x levels.[1–3] Typical strategies for obtaining low NO_x levels from these combustors include tailoring the inlet swirl distribution and the local fuel–air ratio distribution. This is a complicated parametric optimization problem, which can be difficult to tackle efficiently using experiments or, more recently, three-dimensional numerical simulations. Further, although much research has been devoted to this area, the degree of complexity is such that application-specific experimental and numerical studies often lend little physical insight,[4–8] which leads to difficulties when developing new combustors for advanced gas turbine engines.

The objective of this paper is to illustrate the global features of swirling flows with combustion to clarify and understand the behavior of primary zone flows in LPP gas turbine combustors. The approach taken was to develop a quasi-one-dimensional differential control volume model, with a set of influence coefficients that describe the local behavior of the flow. Examination of the influence coefficients, coupled with parametric studies using the one-dimensional model, enabled the effects of swirl, heat release, mixing, and area change to be quantified. A limited assessment of the applicability of the simplified model to flows of interest was carried out through comparison to an axisymmetric Navier–Stokes code as a necessary step in supporting the utility of the results.

The paper begins with a description of the quasi-one-dimensional control volume model in Sec. II followed by presentation and discussion of the influence coefficients derived from the model in Sec. III. Parametric studies using the quasi-one-dimensional model are then presented in Sec. IV. Section V presents a comparison of the quasi-one-dimensional results with Navier–Stokes computations, and Sec. VI gives a summary and conclusions.

II. Quasi-One-Dimensional Model

The quasi-one-dimensional differential control volume model developed is an extension of the work of Darmofal et al.,[9] which focused on the behavior of confined vortex cores in pressure gradients with no heat release or mixing. Through comparison with axisymmetric Navier–Stokes simulations, they showed that the simplified

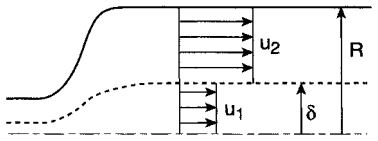

Fig. 1 Quasi-one-dimensional model.

model could be used to predict the onset of recirculation zone formation.

Here we consider a more general case of a vortex core in a duct of varying area, which includes heat release in the core and outer flow and mixing between the streams. The derivation of the equations, which follows from and extends that of Khan,[10] is described in Secs. II.A and II.B.

A. Assumptions

Figure 1 shows a schematic of the model flowfield, which is taken to be axisymmetric, steady, and smoothly varying in the axial direction. A cylindrical coordinate system $\boldsymbol{x} = (r, \theta, z)$ with velocity components $\boldsymbol{u} = (w, v, u)$ is used. The flowfield is divided into a vortex core of radius $\delta(z)$ containing all of the axial vorticity (stream 1) and an irrotational outer flow (stream 2). The duct radius $R(z)$ is specified.

The swirl velocity is taken to be a Rankine vortex

$$v(r, z) = \begin{cases} (\Gamma/2\pi\delta)r/\delta & 0 \le r \le \delta \\ \Gamma/2\pi r & \delta \le r \le R \end{cases} \tag{1}$$

This is not a fundamental limitation of the model; other distributions may be specified; however, LPP combustor inlet data suggests that this profile is an appropriate approximation for many flows of interest.[11] The radial velocity is assumed negligible in the quasi-one-dimensional formulation, and so the radial momentum equation reduces to

$$\frac{\partial p}{\partial r} = \rho\frac{v^2}{r} \tag{2}$$

Axial velocities in the two streams are assumed constant over an axial cross section, although the axial velocities are not necessarily the same in each stream. This implies infinitely fast mixing within each stream to enforce uniform profiles. This intrastream mixing is not the same as the interstream mixing, or mixing between the streams, which can be specified in the model.

B. Conservation Equations

The application of conservation of mass, momentum, and energy, as well as the state equation and a summation of areas to the two streams, yields a system of differential equations. Conservation of mass for streams 1 and 2 can be expressed as

$$\frac{\mathrm{d}\rho_1}{\rho_1} + \frac{\mathrm{d}u_1}{u_1} + \frac{\mathrm{d}A_1}{A_1} = 0 \tag{3}$$

$$\frac{\mathrm{d}\rho_2}{\rho_2} + \frac{\mathrm{d}u_2}{u_2} + \frac{\mathrm{d}A_2}{A_2} = 0 \tag{4}$$

Conservation of momentum for the two streams gives

$$\frac{\mathrm{d}u_1}{u_1} + \frac{\mathrm{d}p_c}{\rho_1 u_1^2} - \frac{1}{2}\Omega^2\frac{\mathrm{d}A_1}{A_1} = \frac{\mathrm{d}\mathcal{M}}{\dot{m}_1 u_1} \tag{5}$$

$$\frac{\mathrm{d}u_2}{u_2} + sr^2\frac{\mathrm{d}p_c}{\rho_1 u_1^2} - \frac{1}{2}(s+1)r^2\Omega^2\frac{\mathrm{d}A_1}{A_1} + \frac{1}{2}sr^2\Omega^2\left(\frac{\alpha}{\alpha-1}\right)\frac{\mathrm{d}\rho_1}{\rho_1} + \frac{1}{2}r^2\Omega^2\left(\frac{\alpha - \ell n\,\alpha}{\alpha-1}\right)\frac{\mathrm{d}\rho_2}{\rho_2} = \frac{-sr^2}{\alpha-1}\frac{\mathrm{d}\mathcal{M}}{\dot{m}_1 u_1} \tag{6}$$

where the different quantities are defined in the Nomenclature. The terms containing area and density differentials that appear on the left-hand side of Eqs. (5) and (6) reflect the effect of the swirl component of velocity. The source term on the right-hand side of the equations represents the transfer of momentum from one stream to the other due to mixing.

Conservation of energy for the two streams yields

$$\frac{\mathrm{d}T_1}{T_1} + \frac{u_1^2}{C_{p1}T_1}\frac{\mathrm{d}u_1}{u_1} = \frac{\mathrm{d}h_{\mathrm{pr}_1}}{C_{p1}T_1} + \frac{\mathrm{d}h_m}{C_{p1}T_1} \tag{7}$$

$$\frac{\mathrm{d}T_2}{T_2} + \frac{u_2^2}{C_{p2}T_2}\frac{\mathrm{d}u_2}{u_2} = \frac{\mathrm{d}h_{\mathrm{pr}_2}}{C_{p2}T_2} - \frac{sr\eta\tau}{\alpha-1}\frac{\mathrm{d}h_m}{C_{p1}T_1} \tag{8}$$

The source terms on the right-hand side of the equations represent the enthalpy addition due to combustion ($\mathrm{d}h_{\mathrm{pr}}$) and the transfer of enthalpy from one stream to the other due to mixing ($\mathrm{d}h_m$).

The equation of state for the two streams is

$$\frac{\mathrm{d}p_c}{p_c} - \frac{\mathrm{d}\rho_1}{\rho_1} - \frac{\mathrm{d}T_1}{T_1} = 0 \tag{9}$$

$$\frac{\mathrm{d}p_c}{p_c} - \frac{\mathrm{d}\rho_2}{\rho_2} - \frac{\mathrm{d}T_2}{T_2} = 0 \tag{10}$$

Summation of areas yields

$$\frac{1}{\alpha}\frac{\mathrm{d}A_1}{A_1} + \frac{\alpha-1}{\alpha}\frac{\mathrm{d}A_2}{A_2} = \frac{\mathrm{d}A_D}{A_D} \tag{11}$$

For the parametric studies presented, the duct radius was specified by the function

$$R(z) = a[\mathrm{erf}(bz - c) + 1] + R_0 \tag{12}$$

where a, b, and c were chosen to give a geometry typical of gas turbine combustors.[12] The values of a, b, and c are 0.02, 60, and 2.5, respectively. Again, the form of Eq. (12) provides a convenient expression, but other forms may be used to address other geometries.

Heat release profiles $\mathrm{d}h_{\mathrm{pr}_i}(z)$ are also specified for both streams, with profiles representative of those found in modern combustors. The total heat release in each stream relative to the incoming flow enthalpy is set to represent a methane–air reaction of the form

$$\mathrm{CH_4} + (2/\phi_i)(\mathrm{O_2} + 3.76\mathrm{N_2}) \rightarrow \mathrm{CO_2} + 2\mathrm{H_2O} + [(2/\phi_i) - 2]\mathrm{O_2} + (7.52/\phi_i)\mathrm{N_2} \tag{13}$$

where ϕ_i is the equivalence ratio of stream i.

The heat release profile is taken the same for both streams except for the value of the peak, which is set by ϕ_i. The profile is given by the function

$$\mathrm{d}h_{\mathrm{pr}_i} = \phi_i\,\mathrm{d}h_{\max}\left(\left\{\mathrm{erf}[d(z/L)] + \tfrac{1}{2}\mathrm{erfc}[e(z/L) - f]\right\} - 1\right) \tag{14}$$

where d, e, and f have been chosen to give heat release profiles typical of gas turbine combustors.[13] For all computations, $L/R_0 = 5$, $d = 14$, $e = 7$, and $f = 3$. Figure 2 shows heat release profiles for low and high heat release cases ($\phi = 0.2$ and 0.8) along with the duct geometry. Consequences of varying the functional form of the heat release profiles and duct geometry were not evaluated in the current study, and only effects of the overall level of heat release were investigated.

Mixing creates the exchange of momentum and energy between the two streams. A mixing coefficient Ξ is specified, where Ξ is a fraction of the mixing rate set by an effective turbulent viscosity ν_t. The mixing rate is thus proportional to $\Xi\,\nu_t$ where ν_t is determined using Prandtl's second hypothesis[14,15]

$$\nu_t = C_1(b'\bar{U})^2(z/\bar{U}) \tag{15}$$

and where b' is defined as[16]

$$b' = \frac{0.37(1-r)\left(1 + s^{\frac{1}{2}}\right)}{2\left(1 + s^{\frac{1}{2}}r\right)}B$$

$$B = 1 - \frac{\left(1 - s^{\frac{1}{2}}\right)}{\left(1 + s^{\frac{1}{2}}\right)\{1 + 2.9[(1+r)/(1-r)]\}} \tag{16}$$

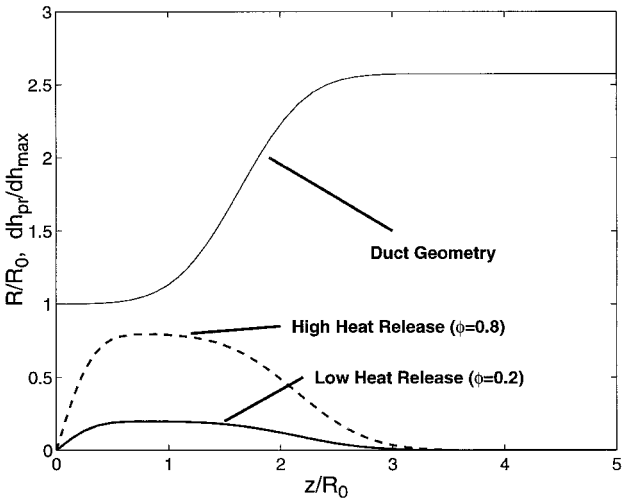

Fig. 2 Heat release and duct radius profiles.

The constant C_1 in Eq. (15) is found by assuming an error function for the velocity profile across the shear layer and using the 5 and 95% points to compute C_1, yielding a value of $C_1 = 0.092$.

The momentum transfer term $d\mathcal{M}/\dot{m}_1 u_1$ can, thus, be expressed as

$$\frac{d\mathcal{M}}{\dot{m}_1 u_1} = -\frac{1}{Re_b}\frac{\rho_1 + \rho_2}{\rho_1}\frac{(u_1 - u_2)^2}{u_1^2}\frac{1}{\delta} \tag{17}$$

and the energy transfer term can be related to the momentum transfer term by

$$\frac{dh_m}{C_{p_1} T_1} = \frac{r}{r-1}\left(\frac{1}{Pr_t}\frac{\tau - 1}{\tau} + E\right)\frac{d\mathcal{M}}{\dot{m}_1 u_1} \tag{18}$$

Again, no effort was made to study the consequences of varying the functional form of the momentum and energy exchange. Only the sensitivity of the model results to the overall mixing rate, ν_t, was investigated. These results are discussed in Sec. IV.

Equations (3–11) are solved by specifying inlet conditions, duct geometry, heat release profiles, and mixing rate and then integrating along the duct in the axial direction. The equations are, thus, parabolic and downstream influences are not felt. This assumption has been investigated by Darmofal et al.[9] for the case without heat addition and mixing, where it was shown, through comparison with solutions from a Navier–Stokes code, that a quasi-one-dimensional model can capture the overall features of the flow, including the tendency for recirculation zone formation.

III. Influence Coefficients

Influence coefficients represent the sensitivity of various flow parameters (dependent variables) to changes in area, heat addition, and mixing (independent variables). Their utility lies not only in quantitative results, but also in the insight they afford into the roles that various mechanisms play in determining the flow behavior. Based on the preceding formulation [Eqs. (1–18)] influence coefficients for two streams with area change, heat release, and mixing have been derived following the method developed by Shapiro and Hawthorne[17] and popularized by Shapiro.[18]

There are several features about the flows of interest that lead to simplifications in the influence coefficient analysis compared to the full set of equations [Eqs. (3–11)]. First, as is the case in gas turbine combustors, the Mach numbers are low enough that changes in pressure have no significant effect on density, and the state equation is, thus, $\rho T \approx \text{const} + \mathcal{O}(M^2)$. (This assumption implies that the quantity $dp/p \approx 0$; the quantity $dp/\rho u^2$ is not zero.) Density variations are, thus, due only to heat release. Further, kinetic energy changes are also small compared to enthalpy changes. Equations (7–10) then simplify to

$$\frac{dT_1}{T_1} = \frac{dh_{pr_1}}{C_{p_1} T_1} + \frac{dh_m}{C_{p_1} T_1} \tag{19}$$

$$\frac{dT_2}{T_2} = \frac{dh_{pr_2}}{C_{p_2} T_2} - \frac{sr\eta\tau}{\alpha - 1}\frac{dh_m}{C_{p_1} T_1} \tag{20}$$

$$\frac{d\rho_1}{\rho_1} + \frac{dT_1}{T_1} = 0 \tag{21}$$

$$\frac{d\rho_2}{\rho_2} + \frac{dT_2}{T_2} = 0 \tag{22}$$

respectively. The influence coefficients are summarized in the Appendix. Note that the influence coefficients collapse to the results of Shapiro[18] for a single stream with no swirl at low Mach number.

As with the full set of equations, Eqs. (3–6), (11), and (19–22) can be interpreted to yield a complete nonlinear solution. Their greatest practical use, however, is to indicate the directions and rates of change of flow variables locally. This type of analysis provides a pathway for understanding complex fluid behavior over a broad parametric range.

The trends derived from the influence coefficients are summarized in Table 1. It should be mentioned that these trends are not dependent on the prescribed geometry, heat release profile, or mixing rate profile because the influence coefficients only describe the local flow behavior based on local ratios of flow variables.

As an example of the use of the influence coefficients, we can examine the change in core axial velocity (du_1/u_1) as a function of heat release in the core ($dh_{pr_1}/C_{p_1} T_1$). We focus on this example for two reasons. First, acceleration or deceleration of the vortex core is directly related to the potential for recirculation zone formation, and many combustors rely on a recirculation zone for flame stability. Second, this situation illustrates a result that may seem counterintuitive and appears to us to be difficult to arrive at with more complex analyses or experiments. Thus, it demonstrates the utility of the simplified model.

The relation between the core axial velocity and the core heat release is given by

$$\frac{du_1}{u_1} = \frac{1 - \frac{1}{2}r^2\Omega^2\left[\alpha(s+1) - 1\right]}{\beta}\frac{dh_{pr_1}}{C_{p_1} T_1} \tag{23}$$

where β is defined as

$$\beta = 1 + r^2(\alpha - 1)\left(s - \tfrac{1}{2}\Omega^2\right) \tag{24}$$

Examining the denominator of the influence coefficient [Eq. (23)], the local swirl ratio Ω that yields $\beta = 0$ can be found. This swirl ratio, Ω_{crit}, defined as

Table 1 Local trends from influence coefficients

Parameter	Duct area change	Heat release in core	Heat release in outer flow	Mixing (2 → 1)
p_c	↑	↓, $\Omega < \Omega_2$ ↑, $\Omega > \Omega_2$	↓	↑
u_1	↓	↑, $\Omega < \Omega_1$ ↓, $\Omega > \Omega_1$	↑	↓
u_2	↓, $\Omega < \Omega_3$ ↑, $\Omega > \Omega_3$	↑	↑	↑
A_1	↑	↑	↓	↓
A_2	↑, $\Omega < \Omega_3$ ↓, $\Omega > \Omega_3$	↓	↑	↑
p_{t_1}	No effect	↓	No effect	↑
p_{t_2}	No effect	No effect	↓	↓

$$\Omega_{\text{crit}} = \sqrt{2\left(s + \frac{1}{r^2(\alpha - 1)}\right)} \tag{25}$$

corresponds to the critical value of swirl ratio at which (locally) the core growth rate is unbounded. This is of interest because this condition has been linked to recirculation zone formation.[9] In the following discussion, only swirl ratios below critical will be considered.

When Eq. (23) is examined again and the swirl ratio that makes the numerator of the influence coefficient zero is solved for, a local swirl ratio is found where the sign of the influence coefficient changes. This corresponds to a reversal of the effect of adding heat to the core. Specifically, for low swirl ratios, adding heat to the core accelerates the core, as is familiar from the limiting case of zero swirl. At high swirl ratios, however, adding heat to the core decelerates the core. This transitional swirl ratio between the two regimes is denoted as Ω_1 in Table 1 and defined as

$$\Omega_1 = \sqrt{\frac{2}{r^2[\alpha(s + 1) - 1]}} \tag{26}$$

Note that Ω_1 is a function of the local ratios of density, velocity, and area only. Thus, from the perspective of combustor design, it is possible for particular choices of local fuel–air ratio and swirler geometry to lead to acceleration or deceleration of the vortex core, thereby hindering or promoting recirculation zone formation.

A physical explanation for the described behavior can be given as follows. Consider the cases of no swirl and strong swirl for a vortex core in a constant area duct, where strong swirl means a swirl ratio just below the critical swirl ratio. For simplicity, we assume the core and outer flow to have the same value of axial velocity upstream of the region of heat addition, although this is not necessary for the arguments that follow.

Consider the no-swirl situation first. Heat addition will lower the density and cause the core to expand, as shown in Fig. 3a. The streamtube area in the outer flow thus contracts, so that the outer flow axial velocity increases and the static pressure decreases in the flow direction. Because the static pressure is uniform across the duct, this implies an acceleration in the core ($\rho u\, \mathrm{d}u = -\mathrm{d}p$).

Consider now the situation of strong swirl, so that the effect of the change in axial velocity on static pressure is small. Again, as shown in Fig. 3b, the core expands in the region of heat addition. At the outer radius of the duct, i.e., at the wall, the azimuthal velocity and the stagnation pressure do not vary along the duct. Radial equilibrium, thus, implies that in the axial region in which there is heat addition, and therefore core expansion, the static pressure on the interface between the two streams will increase in the direction of the flow. Thus, there is a pressure force pointing upstream on a volume of the vortex core between stations upstream and downstream of the heat addition and, hence, a deceleration of the core.

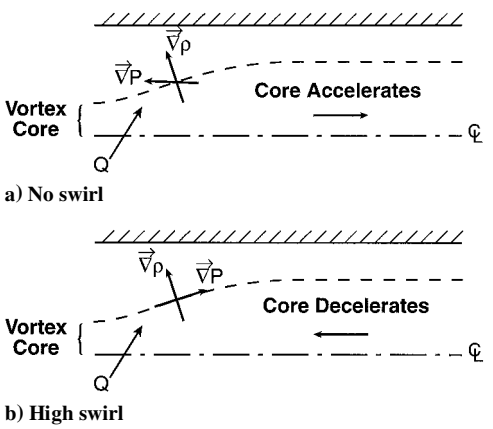

Fig. 3 Schematic of circulation generation due to baroclinic torque for no swirl and high swirl.

The physical basis for the described behavior can also be viewed from the perspective of vorticity dynamics. Changes in the azimuthal vorticity, i.e., vorticity oriented in the θ direction, at the edge of the core, are set by a balance between the production of negative azimuthal vorticity due to stretching and the production of positive azimuthal vorticity due to baroclinic torque. Stretching of the interface occurs due to dilatation of the gas in the core, whereas the baroclinic torque occurs due to nonparallel pressure and density gradients. A net production of negative azimuthal vorticity corresponds to a deceleration of the core. A net production of positive azimuthal vorticity corresponds to an acceleration of the core.

Examining the influence coefficients further, two more swirl ratios can be defined where other coefficients change sign. These two, denoted as Ω_2 and Ω_3, define the boundaries between the low and high swirl behavior of centerline static pressure with heat release in the core and outer stream velocity/area with duct area change. The swirl ratios Ω_2 and Ω_3 are defined as

$$\Omega_2 = \sqrt{\frac{-r^2[(\alpha - 1) + s(2\alpha - 1)] + F}{\alpha s r^2}} \tag{27}$$

and

$$\Omega_3 = \sqrt{2s} \tag{28}$$

where F is given by

$$F = \sqrt{r^4[(\alpha - 1) + s(2\alpha - 1)]^2 + 4\alpha s r^2}$$

As shown in Table 1, several other statements can be made as to the effect of area change, heat release, and mixing on recirculation zone formation. A decrease in core axial velocity moves the flow toward the formation of a recirculation zone, whereas an increase in core axial velocity moves the flow away from the formation of a recirculation zone. Thus, an increase in duct area enhances recirculation zone formation, as expected. Heat release in the outer flow hinders recirculation zone formation, as does mixing between the streams (defined as positive for exchange of momentum and energy from the outer flow to the core). Finally, there are no regions where the behavior changes with swirl for heat release in the outer flow or for mixing between the streams.

IV. Results of Quasi-One-Dimensional Analysis

The local trends given by the influence coefficients were examined for the whole duct flowfield by using the solution from the one-dimensional model to calculate values of Ω_1, Ω_2, Ω_3, and Ω_{crit}. These values are compared to the local swirl ratio (Ω) given by the solution from the quasi-one-dimensional code to determine the behavior of the flow in a given section of the duct. Figure 4a shows the results from a high swirl, low heat release case ($\phi_1 = \phi_2 = 0.2$), whereas Fig. 4b shows the results from a high swirl, high heat release case ($\phi_1 = \phi_2 = 0.8$). The values of the inlet parameters for these runs are given in Table 2.

In Fig. 4, the solution from the quasi-one-dimensional model (Ω) is denoted by the asterisks, and six regions are defined, labeled 1–6. The boundaries of these regions are the swirl ratios where the influence coefficients, given in the Appendix, change sign. These swirl ratios, defined by Eqs. (26–28) and denoted by the solid, dashed, and dashed–dot lines, respectively, have been computed using the solution from the quasi-one-dimensional model. The other boundary on Fig. 4 is the critical swirl ratio defined by Eq. (25) and denoted by

Table 2 Conditions for the high swirl cases of Fig. 4

Inlet parameter	Value
Swirl ratio, Ω_0	1.5
Velocity ratio, r_0	0.8
Density ratio, s_0	1
Area ratio, α_0	4

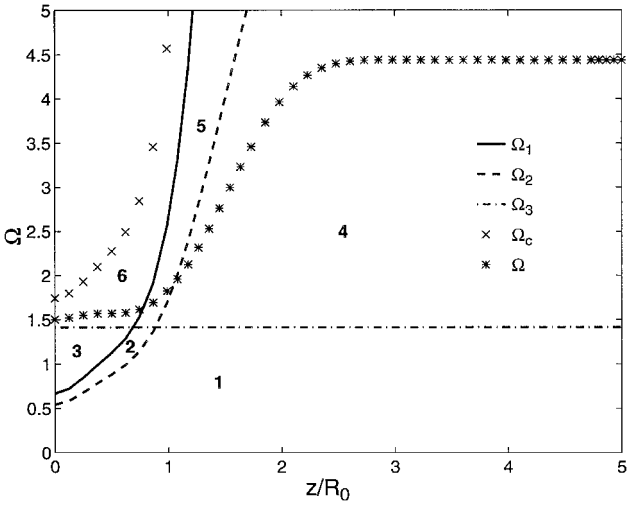

a) Low heat release ($\phi_1 = \phi_2 = 0.2$)

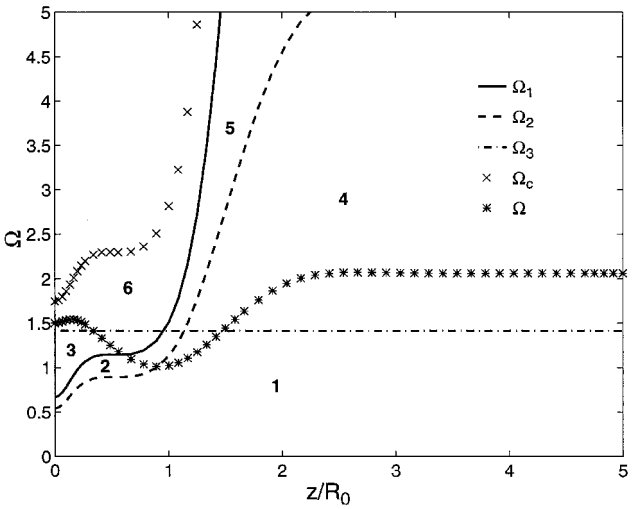

b) High heat release ($\phi_1 = \phi_2 = 0.8$)

Fig. 4 Flow regime maps for high swirl ($\Omega_0 = 1.5$).

the ×. It corresponds to the conditions where the influence coefficients go to $\pm\infty$.

The behavior of the flow at any axial location in the duct is determined by which region the solution (Ω) lies in at that point. Region 1 is below all of the boundaries, and the behavior of the flow is qualitatively similar to the zero swirl behavior. Region 2 is above the dashed line, meaning that the local swirl ratio (Ω) is greater than Ω_2. This corresponds, as is shown in Table 1, to the case where adding heat to the core increases the centerline static pressure, counter to the low swirl behavior. Region 3 lies above both the solid and dashed lines (Ω_1 and Ω_2, respectively), and so adding heat to the core increases the centerline static pressure and decelerates the core, as shown in Table 1.

In region 4, adding heat to the core accelerates the core and decreases the centerline static pressure as in the zero swirl case. However, increasing the duct area increases the axial velocity of the outer stream and decreases the area of the outer stream. This effect, shown in Table 1, is again counter to the zero swirl case. In region 5, adding heat to the core increases the centerline static pressure, whereas increasing the duct area increases the outer stream axial velocity and decreases the outer stream area. Finally, in region 6, adding heat to the core increases the centerline static pressure and decreases the core axial velocity, whereas increasing the duct area increases the outer stream axial velocity and decreases the outer stream area. All of these effects are summarized in Table 1.

By comparing the low and high heat release cases of Figs. 4a and 4b, respectively, we can see that the shape of the six regions changes somewhat as does the trajectory of the solution (*s), although the solution begins and ends in the same regions. Plotting the solution in this manner is useful for understanding the parametric behavior. Examination of the solution and its relation to the boundaries for trend reversal given by the influence coefficients allows the determination of the effect of heat release for a given set of inlet conditions, heat release profiles, and geometry.

Note that at no point in either Figs. 4a or 4b does the local swirl ratio approach the critical swirl ratio Ω_{crit}. A case was computed with a duct-to-core area ratio of 100 instead of 4 and showed a significant growth of the core as the local swirl ratio approached critical. This rapid and large core growth, along with a concurrent drop in core axial velocity toward zero, indicates the onset of reverse flow and, hence, recirculation zone formation. However, the reversed flow case is not handled by the current model, and therefore, only a solution with the swirl ratio approaching, not reaching, critical can be studied. The likelihood of recirculation zone formation is greatly increased for larger initial area ratios. This corresponds to starting with a smaller vortex core for a given initial duct geometry. Therefore, as the initial area of the vortex decreases for a given initial duct area, more room exists for the core to expand. This allows the centerline velocity to approach zero, thereby increasing the potential for recirculation zone formation. This result is consistent with the results of Darmofal et al.[9]

When we turn now to the effect of interstream mixing, it can be seen from Table 1 that no regions exist where the trends change due

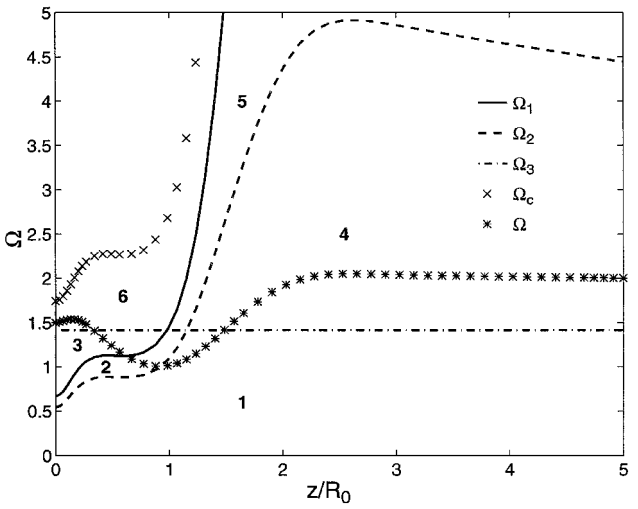

a) Low mixing rate (ν_t)

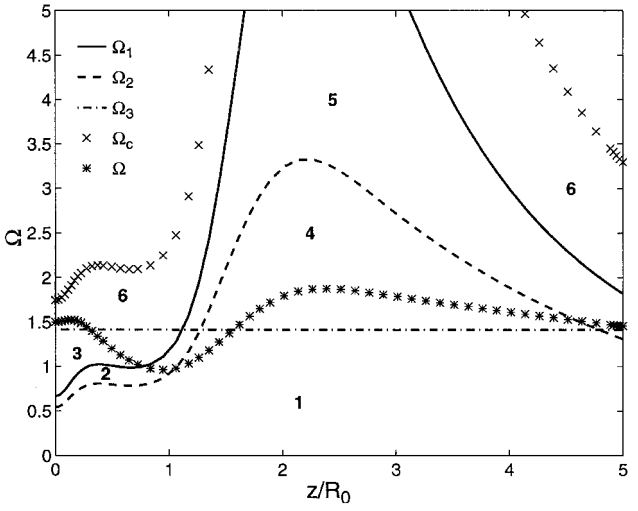

b) High mixing rate ($10\nu_t$)

Fig. 5 Flow regime maps for high swirl ($\Omega_0 = 1.5$) and high heat release ($\phi_1 = \phi_2 = 0.8$).

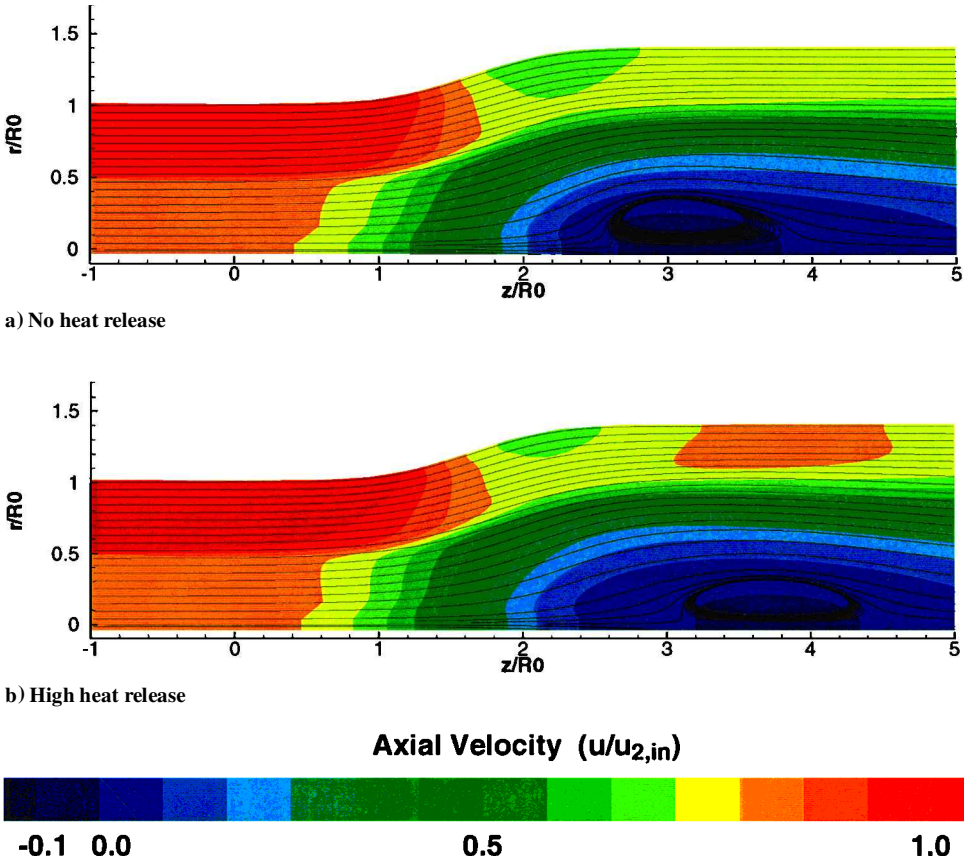

a) No heat release

b) High heat release

Fig. 6 Axial velocity contours and streamlines for a Navier–Stokes case with low swirl and varying heat release.

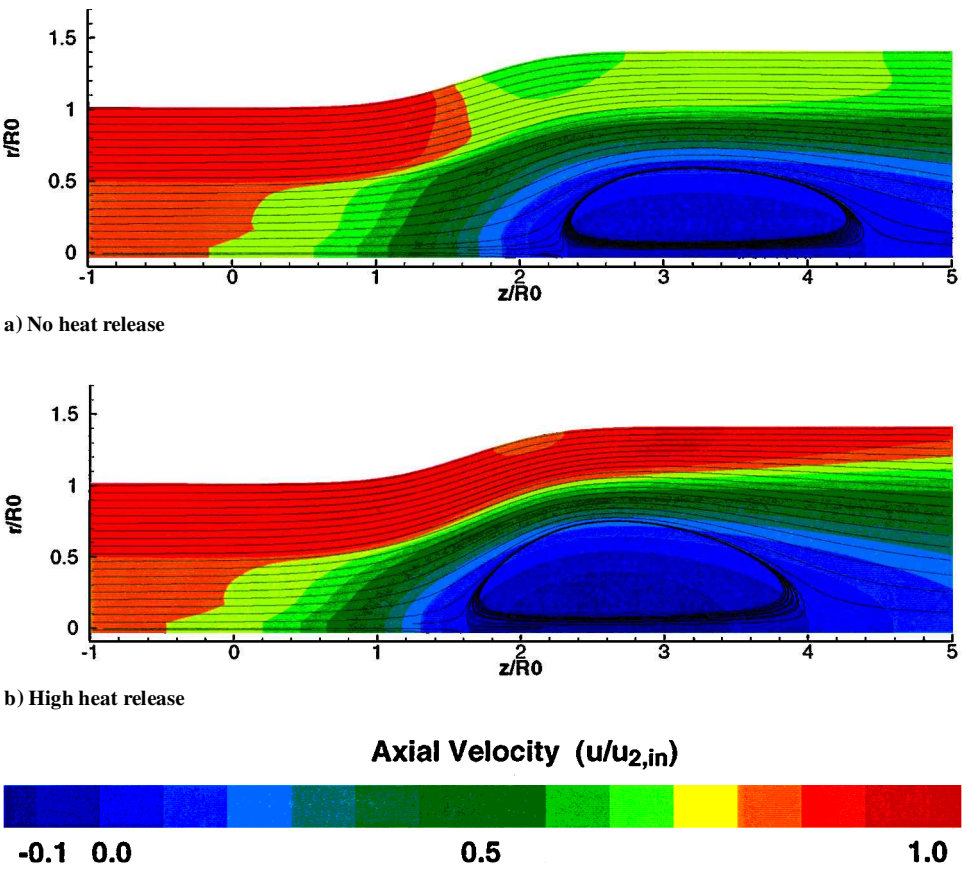

a) No heat release

b) High heat release

Fig. 7 Axial velocity contours and streamlines for a Navier–Stokes case with high swirl and varying heat release.

Table A1 Influence coefficients for two streams with area change, heat release, and mixing[a]

Coefficient	$\frac{dA_D}{A_D}$	$\frac{dh_{pr_1}}{C_{p_1}T_1}$	$\frac{dh_{pr_2}}{C_{p_2}T_2}$	$\frac{d\mathcal{M}}{\dot{m}_1 u_1}$
$\frac{dp_c}{\rho_1 u_1^2}$	$\frac{\alpha\left(1+\frac{1}{2}\Omega^2\right)}{\beta}$	$-\frac{1-\frac{1}{2}r^2\Omega^2\left[(\alpha-1)+s\left(2\alpha+\frac{1}{2}\alpha\Omega^2-1\right)\right]}{\beta}$	$-\frac{\left(1+\frac{1}{2}\Omega^2\right)\left[(\alpha-1)-\frac{1}{2}r^2\Omega^2(\alpha-\ell_n\alpha)\right]}{\beta}$	$\frac{1-sr^2-\frac{1}{2}r^2\Omega^2[\alpha(s+1)-1]}{\beta}-\epsilon\frac{1-\alpha sr^2\Omega^2-\frac{1}{2}r^2\Omega^2[(\alpha-1)-s\left(1-\frac{1}{2}\alpha\Omega^2\right)]-\left(1+\frac{1}{2}\Omega^2\right)\eta\tau G}{\beta}$
$\frac{du_1}{u_1}$	$-\frac{\alpha}{\beta}$	$\frac{1-\frac{1}{2}r^2\Omega^2[\alpha(s+1)-1]}{\beta}$	$\frac{(\alpha-1)-\frac{1}{2}r^2\Omega^2(\alpha-\ell_n\alpha)}{\beta}$	$\frac{\alpha sr^2}{\beta}+\epsilon\frac{1-\frac{1}{2}r^2\Omega^2[\alpha(s+1)-1]-\eta\tau G}{\beta}$
$\frac{du_2}{u_2}$	$-\frac{\alpha r^2\left(s-\frac{1}{2}\Omega^2\right)}{\beta}$	$sr^2\left(1+\frac{1}{2}\frac{\alpha}{\alpha-1}\Omega^2\right)\Big/\beta$	$r^2\left[(\alpha-1)\left(s-\frac{1}{2}\Omega^2\right)+\frac{1}{2}\Omega^2\left(\frac{\alpha-\ell_n\alpha}{\alpha-1}\right)\right]\Big/\beta$	$-\frac{sr^2\alpha/(\alpha-1)}{\beta}+\epsilon\left\{\frac{sr^2\left[1-\frac{1}{2}\alpha r^2\Omega^2\left(s-\frac{1}{2}\Omega^2\right)\right]-r^2\left(s-\frac{1}{2}\Omega^2\right)\eta\tau G}{\beta}+J+K\right\}$
$\frac{dT_1}{T_1}$	0	1	0	ϵ
$\frac{dT_2}{T_2}$	0	0	1	$-\frac{sr\eta\tau}{\alpha-1}\epsilon$
$\frac{d\rho_1}{\rho_1}$	0	-1	0	$-\epsilon$
$\frac{d\rho_2}{\rho_2}$	0	0	-1	$\frac{sr\eta\tau}{\alpha-1}\epsilon$
$\frac{dA_1}{A_1}$	$\frac{\alpha}{\beta}$	$\frac{(\alpha-1)sr^2+\frac{1}{2}\alpha sr^2\Omega^2}{\beta}$	$-\frac{(\alpha-1)-\frac{1}{2}r^2\Omega^2(\alpha-\ell_n\alpha)}{\beta}$	$-\frac{\alpha sr^2}{\beta}+\epsilon\frac{(\alpha-1)sr^2+\frac{1}{2}\alpha sr^2\Omega^2+\eta\tau G}{\beta}$
$\frac{dA_2}{A_2}$	$\frac{\alpha r^2\left(s-\frac{1}{2}\Omega^2\right)}{\beta}$	$-\left[sr^2\left(1+\frac{1}{2}\frac{\alpha}{\alpha-1}\Omega^2\right)\Big/\beta\right]$	$\left[1-\frac{1}{2}r^2\Omega^2\left(\frac{\alpha-\ell_n\alpha}{\alpha-1}\right)\Big/\beta\right]$	$\frac{sr^2\alpha/(\alpha-1)}{\beta}-\epsilon\left\{\frac{sr^2\left[1-\frac{1}{2}\alpha r^2\Omega^2\left(s-\frac{1}{2}\Omega^2\right)\right]-r^2\left(s-\frac{1}{2}\Omega^2\right)\eta\tau G}{\beta}+J+L\right\}$
$\frac{dp_{t_1}}{\rho_1 u_1^2}$	0	$-\frac{1}{2}(1+\Omega^2)$	0	$1-\frac{1}{2}(1+\Omega^2)\epsilon$
$\frac{dp_{t_2}}{\rho_2 u_2^2}$	0	0	$-\frac{1}{2}(1+\Omega^2)$	$-sr^2/(\alpha-1)+\frac{1}{2}(1+\Omega^2)[sr\eta\tau/(\alpha-1)]\epsilon$

[a] $G = sr-\frac{1}{2}sr^3\Omega^2(\alpha-\ell_n\alpha)$, $\epsilon = [r/(r-1)]\{1/Pr_t[(\tau-1)/\tau]+E\}$, $J = \frac{1}{2}[\alpha/(\alpha-1)]sr^2\Omega^2$, $K = \frac{1}{2}sr^3\Omega^2[(\alpha-\ell_n\alpha)/(\alpha-1)]\eta\tau/(\alpha-1)$, $L = [sr\eta\tau/(\alpha-1)]\{1-\frac{1}{2}r^2\Omega^2[(\alpha-\ell_n\alpha)/(\alpha-1)]\}$.

to mixing. Therefore, the addition of mixing only modifies the shape of the various flow regimes. Figure 5 shows two flow regime maps for a high swirl ($\Omega = 1.5$), high heat release ($\phi_1 = \phi_2 = 0.8$) case with different mixing rates. The mixing rate for Fig. 5a was chosen to be equal to that predicted by the planar shear layer growth rate of Hermanson and Dimotakis.[16] The mixing rate for Fig. 5b was chosen to be 10 times that mixing rate.

When we compare Figs. 4b and 5a, it is seen that there is little difference between the no mixing case and the low mixing case. Comparing Figs. 5a and 5b, one sees that the shape of the regions has been altered for the high mixing rate case, but the overall effect on the solution is small. Therefore, mixing does not change the parametric flow behavior. Additional flow maps for a low swirl case with varying heat release and mixing are presented in the thesis by Underwood.[19]

The flow regime maps presented in Figs. 4 and 5 show that although the influence coefficient analysis yields local trends only, these trends can be shown in a global context. Flow regime maps provide a useful tool for viewing regions of differing flow behavior and their relation to the local swirl ratio at a given point in the duct.

V. Comparison with Navier–Stokes Simulations

The quasi-one-dimensional model has been shown to provide insight into the physical processes present in swirling flows with combustion, but we need to define the applicability to the flows of greatest interest, i.e., flows with recirculation. To this end, the quasi-one-dimensional model has been compared with the results from an axisymmetric Navier–Stokes code.

The Navier–Stokes code allows calculation of steady and unsteady reacting flows with recirculation zones.[20] The reaction process is modeled using a flame sheet approximation for premixed combustion with the heat addition calculated consistent with that of a methane–air reaction. As a consequence of the flame sheet approximation, a slip velocity at the wall is allowed because specification of a no-slip wall boundary causes the flame front to propagate upstream to the inlet in the wall boundary layer. Only steady solutions were examined for comparison to the quasi-one-dimensional model.

Comparison of the one-dimensional model and the Navier–Stokes code was carried out for a recirculating case. Heat release was varied for the same inlet conditions to test the validity of the influence coefficients for suggesting trends in flow behavior. Specifically, the low/high swirl behavior with heat release in the core was examined by observing changes in size and location of the recirculation zone for varying heat release. The results are shown in Figs. 6 and 7 for the low and high swirl behaviors, respectively.

A low swirl ($\Omega_0 = 0.5$) case with zero and high heat release ($\phi = 0, 0.8$) is shown in Figs. 6a and 6b, respectively. Contours of axial velocity are plotted along with the streamlines. Figure 6 shows that, for low swirl, increasing heat release causes an acceleration of the streamtube on the centerline, which results in a weaker recirculation zone located farther downstream, as would be expected for the limiting case of no swirl.

A high swirl ($\Omega_0 = 0.8$) case with zero and high heat release ($\phi = 0, 0.8$) is shown in Figs. 7a and 7b, respectively. Figure 7 shows that for high swirl, increasing heat release causes deceleration of the streamtube on the centerline, resulting in a stronger recirculation zone, which is located farther upstream, in accord with the trends from the influence coefficients. These results support the utility of the quasi-one-dimensional model for developing insight into the parametric trends of swirling flows with combustion.

VI. Conclusions

A quasi-one-dimensional analysis including an influence coefficient formulation has been developed to examine the behavior of swirling flows in variable area ducts with heat addition and mixing at conditions representative of LPP combustor flows. The one-dimensional analysis showed that there are regimes where the behavior differs depending on the level of swirl. Comparison with results of a Navier–Stokes code showed that trends for recirculation zone formation suggested by the one-dimensional analysis were borne out by the Navier–Stokes simulations.

Based on the results from the influence coefficients, quasi-one-dimensional model, and Navier–Stokes code, several conclusions can be drawn.

1) For low swirl ratios, heat release in the core hinders recirculation zone formation.

2) For high swirl ratios, heat release in the core enhances recirculation zone formation.

3) For all swirl ratios, heat release in the outer stream hinders recirculation zone formation.

4) Mixing hinders recirculation zone formation.

5) Increasing duct area enhances recirculation zone formation.

6) Vortex cores with a smaller initial area are more susceptible to recirculation zone formation.

Physical mechanisms for these trends have been described.

Appendix: Influence Coefficients

The influence coefficients described in Sec. III are presented in Table A1. They represent the sensitivities of the dependent variables (shown in the leftmost column) to changes in the independent variables (shown in the top row).

Acknowledgments

Support for this work was provided by the Office of Naval Research under ONR Grant N00014-95-1-0592 with Gabriel D. Roy as Technical Monitor. This support is gratefully acknowledged. The authors would like to thank F. E. Marble of the California Institute of Technology, N. A. Cumpsty of Cambridge University, W. A. Sowa of the United Technologies Research Center, and S. A. Syed of Pratt and Whitney, United Technologies Corporation, for their stimulating discussions and insightful suggestions. In addition, the authors would like to thank G. Hendricks and D. Choi of the United Technologies Research Center for their expertise in modifying and running the axisymmetric Navier–Stokes code.

References

[1] Gupta, A. K., Beér, J. M., and Swithenbank, J., "Concentric Multi-Annular Swirl Burner: Stability Limits and Emission Characteristics," *Sixteenth Symposium (International) on Combustion*, Combustion Inst., Pittsburgh, PA, 1976, pp. 79–91.

[2] Gupta, A. K., Modarres-Razavi, M. R., and Marchionna, N., "Experimental and Theoretical Studies in the Controlled Mixing Variable Geometry Combustor," AIAA Paper 88-2857, July 1988.

[3] Gupta, A. K., Ramavajjala, M., and Taha, M., "The Effect of Swirl and Nozzle Geometry on the Structure of Flames and NO_x Emission," AIAA Paper 92-0766, Jan. 1992.

[4] Johnson, B. V., Roback, R., and Bennett, J. C., "Scalar and Momentum Turbulent Transport Experiments with Swirling and Nonswirling Flows," *Experimental Measurements and Techniques in Turbulent Reactive and Nonreactive Flows Meeting*, *Proceedings of the Winter Annual Meeting*, American Society of Mechanical Engineers, New York, 1984, pp. 107–119.

[5] Milosavljevic, V. D., Taylor, A. M. K. P., and Whitelaw, J. H., "The Influence of Burner Geometry and Flow Rates on the Stability and Symmetry of Swirl-Stabilized Nonpremixed Flames," *Combustion and Flame*, Vol. 80, May 1990, pp. 196–208.

[6] Anderson, L. R., Heiser, W. H., and Jackson, J. C., "Axisymmetric One-Dimensional Compressible Flow-Theory and Applications," *ASME Journal of Applied Mechanics*, Vol. 37, No. 4, Dec. 1970, pp. 917–923.

[7] Bicen, A. F., Tse, D. G. N., and Whitelaw, J. H., "Combustion Characteristics of a Model Can-Type Combustor," *Combustion and Flame*, Vol. 80, May 1990, pp. 111–125.

[8] Koutmos, P., and McGuirk, J. J., "Isothermal Modeling of Gas Turbine Combustors: Computational Study," *Journal of Propulsion and Power*, Vol. 7, No. 6, 1991, pp. 1064–1071.

[9] Darmofal, D. L., Khan, R., Greitzer, E. M., and Tan, C. S., "A Quasi One-Dimensional Model for Vortex Cores," Internal Gas Turbine Lab. Rept. 230, Massachusetts Inst. of Technology, Cambridge, MA, June 1997.

[10] Khan, R., "A Quasi One-Dimensional Analysis for Confined Vortex Cores," M.S. Thesis, Dept. of Aeronautics and Astronautics, Massachusetts Inst. of Technology, Cambridge, MA, June 1995.

[11] Beér, J. M., and Chigier, N. A., *Combustion Aerodynamics*, Krieger, Malabar, FL, 1972, pp. 100–144.

[12] Kerrebrock, J. L., *Aircraft Engines and Gas Turbines*, MIT Press, Cambridge, MA, 1977, pp. 154–179.

[13] Rizk, N. K., and Mongia, H. C., "Gas Turbine Combustor Design Methodolgy," AIAA Paper 86-1531, June 1986.
[14] Schlichting, H., *Boundary Layer Theory*, McGraw-Hill, New York, 1955, pp. 555–595.
[15] Tew, D. E., "Streamwise Vorticity Enhanced Compressible Mixing Downstream of Lobed Mixers," Ph.D. Dissertation, Dept. of Aeronautics and Astronautics, Massachusetts Inst. of Technology, Cambridge, MA, June 1995.
[16] Hermanson, J. C., and Dimotakis, P. E., "Effects of Heat Release in a Turbulent, Reacting Shear Layer," *Journal of Fluid Mechanics*, Vol. 199, Feb. 1989, pp. 333–375.
[17] Shapiro, A. H., and Hawthorne, W. R., "The Mechanics and Thermodynamics of Steady, One-Dimensional Gas Flow," *Journal of Applied Mechanics*, Vol. 14, No. 4, 1947, pp. A-317–A-336.
[18] Shapiro, A. H., *The Dynamics and Thermodynamics of Compressible Fluid Flow*, Ronald, New York, 1953, pp. 219–260.
[19] Underwood, D. S., "Primary Zone Models for Gas Turbine Combustors," Ph.D. Dissertation, Dept. of Aeronautics and Astronautics, Massachusetts Inst. of Technology, Cambridge, MA, June 1999.
[20] Wake, B. E., Choi, D., and Hendricks, G., "Numerical Investigation of Pre-Mixed Step-Combustor Instabilities," AIAA Paper 96-0816, Jan. 1996.

Color reproductions courtesy of Massachusetts Institute of Technology.